High-temperature phase transitions in dense germanium

Liam C. Kelsall, [ID] Miriam Peña-Alvarez, Miguel Martinez-Canales, [ID] Jack Binns, Chris J. Pickard, Philip Dalladay-Simpson, Ross T. Howie, and [ID] Eugene Gregoryanz

View Online   **Export Citation**   **CrossMark**

ARTICLES YOU MAY BE INTERESTED IN

High-temperature phase transitions in dense germanium

View Online   Export Citation   CrossMark

Liam C. Kelsall,[1] Miriam Peña-Alvarez,[1,a] (iD) Miguel Martinez-Canales,[1] Jack Binns,[2,b] (iD) Chris J. Pickard,[3,4]
Philip Dalladay-Simpson,[2] Ross T. Howie,[2] and Eugene Gregoryanz[1,2,5,c] (iD)

AFFILIATIONS

[1] SUPA, School of Physics and Astronomy and CSEC, University of Edinburgh, Peter Guthrie Tait Road, Edinburgh EH9 3FD,
 United Kingdom
[2] Center for High-Pressure Science and Technology Advanced Research, Shanghai, People's Republic of China
[3] Department of Materials Science and Metallurgy, University of Cambridge, Cambridge, United Kingdom
[4] Advanced Institute for Materials Research, Tohoku University, 2-1-1 Katahira, Aoba, Japan
[5] Key Laboratory of Materials Physics, Institute of Solid State Physics, CAS, Hefei, China

[a] Author to whom correspondence should be addressed: mpenaal@ed.ac.uk
[b] Present address: School of Science, RMIT University, Melbourne, Victoria 3000, Australia.
[c] Electronic mail: e.gregoryanz@ed.ac.uk

ABSTRACT

Through a series of high-pressure x-ray diffraction experiments combined with *in situ* laser heating, we explore the pressure–temperature phase diagram of germanium (Ge) at pressures up to 110 GPa and temperatures exceeding 3000 K. In the pressure range of 64–90 GPa, we observe orthorhombic Ge-IV transforming above 1500 K to a previously unobserved high-temperature phase, which we denote as Ge-VIII. This high-temperature phase is characterized by a tetragonal crystal structure, space group $I4/mmm$. Density functional theory simulations confirm that Ge-IV becomes unstable at high temperatures and that Ge-VIII is highly competitive and dynamically stable at these conditions. The existence of Ge-VIII has profound implications for the pressure–temperature phase diagram, with melting conditions increasing to much higher temperatures than previous extrapolations would imply.

Published under license by AIP Publishing. https://doi.org/10.1063/5.0047359

I. INTRODUCTION

The understanding of the group-XIV elements holds importance to both fundamental science and technological applications due to their relative abundance in the Earth and diverse electronic properties that they exhibit.[1–10] The use of germanium (Ge), in particular, was crucial in the early developments of transistors, paving the way for the technology we use today.[5] Although Ge has been supplanted by its lighter group-XIV member, silicon (Si), in many applications, it still holds some advantages due to its higher intrinsic electron mobility and enhanced quantum-confinement effects.[11,12]

Owing to their chemical similarity, Ge and Si are observed to undergo the same sequence of structural transitions during compression at room temperature.[13–16] At ambient pressure and temperature, both Ge-I[14] and Si-I[17] exist in a semi-metallic diamond-type structure ($Fd\bar{3}m$). Upon compression above 7 GPa, Ge-I undergoes

a sluggish transition to Ge-II (Fig. 1), manifested by a tetragonal distortion to the metallic β-Sn type structure ($I4_1/amd$),[18,19] with transition being complete at 12 GPa. This phase exhibits a remarkable stability of 55 GPa range[20] (Fig. 1), compared to the interval of only 2 GPa of Si-II.[17] Above 75 GPa, Ge-II undergoes a displacive transition into the orthorhombic Ge-IV (*Imma*). Ge-IV is stable at 85 GPa,[20] when it transforms to the hexagonal phase Ge-V ($P6/mmm$)[21] (Fig. 1). The analogous *Imma* phase of silicon is Si-XI, which appears between 11.7 and 13.2 GPa[22,23] before transitioning to the hexagonal Si-V above 13.2 GPa.[14,24] Ge-V ($P6/mmm$) is stable only over a narrow pressure interval, transforming to Ge-VI (*Cmca*) at 100 GPa[20] (Fig. 1), which is structurally equivalent to Si-VI, observed at 38 GPa.[25] Ge-VI (*Cmca*) transitions into Ge-VII ($P6_3/mmc$) at 170 GPa,[26] which is analogous to the Si-VII structure observed between 42 and 76 GPa.[14,27] Table S1 summarizes the structural information on Ge and Si.
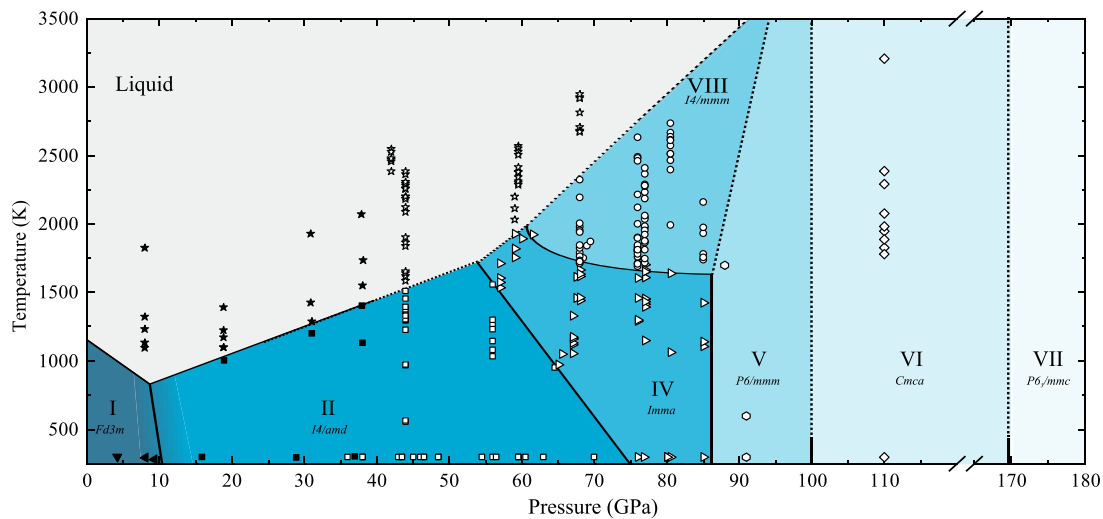
FIG. 1. Proposed phase diagram of Ge up to 180 GPa and 3500 K. Open symbols represent this work and solid symbols represent data from Ref. 28.

Interestingly, Ge does not follow the same structural sequence as Si on decompression; instead, it transforms to new, metastable allotropes.[18,29–32] These phases are highly dependent on the rate of pressure release: fast decompression from β-Sn Ge-II results in the formation of a BC8 structure ($Ia\bar{3}$), which gradually changes to a hexagonal diamond structure ($P6_3/mmc$) at ambient pressure.[33,34] Alternatively, slow decompression from Ge-II leads to the formation of Ge-III, a metastable tetragonal structure ($P4_32_12$).[18,29–32]

Previous high-temperature studies have mapped out the P–T Ge I–II boundary and determined melting temperatures up to 37 GPa[19,28] (see Fig. 1). The melting curve of Ge-I has a negative slope, which ends in the I–II–liquid triple point at ~8.7 GPa and ~833 K.[19] Above this point, the melting temperature increases, reaching ~1500 K by 35 GPa (Fig. 1). Similar behavior is observed in Si, with melting temperatures decreasing for the C-diamond Si-I phase and then increasing in β-Sn Si-II.[35] Despite the rich polymorphism, neither system has experimentally shown to exhibit high-temperature phases.

In this article, we combine high-pressure and high-temperature x-ray diffraction measurements and density functional theory (DFT) calculations to study the phase diagram of germanium in a wide pressure–temperature range. Using double-sided continuous-wave (CW) laser heating in diamond anvil cells, we explore the behavior of Ge up to 115 GPa and 3000 K. Above 65 GPa and 1700 K, we observe that Ge-IV transforms to a previously unknown phase, which we denote here as Ge-VIII. This novel phase is determined to adopt a tetragonal structure (space group $I4/mmm$) and is stable only at high temperatures, reversing to Ge-IV on quenching. This structure has been confirmed in several experimental runs using MgO and H_2 as pressure-transmitting media (PTM). Density functional theory simulations demonstrate that the room temperature Ge-IV is unstable above 1500 K and Ge-VIII is energetically highly competitive and dynamically stable at these conditions. We also explore the P–T space that Ge-VIII covers within the phase diagram and the high-temperature stability of Ge-V and Ge-VI.

II. METHODS

A. Experimental

For these experiments, Boehler-Almax cut diamonds were chosen with 100 μm culets. These diamonds were then used to indent a rhenium gasket to a thickness of 25 μm, in which a 60 μm hole was drilled to act as the sample chamber.

High-purity Ge powder (99.999%, sim 100 mesh, Aldrich) was used. Ge chunks were initially precompressed into foils of ~8 μm thick and loaded into diamond anvil cells (DACs) with the pressure-transmitting medium.

As pressure-transmitting media, we use either MgO (Alfa Aesar, nanopowder, 99+%) or research grade hydrogen (99.9995%, BOC) loaded at 0.2 GPa, as indicated in each discussed run. MgO was used as a pressure medium, as an insulating layer to protect the diamonds during laser heating, and as a pressure marker.[36] The pressure was determined by MgO diffraction patterns[36] and/or diamond edge.[37]

Powder XRD data were collected at the APS, on the GeoSoilEnviroCARS 13IDD beamline, and at the 16-IDB High Pressure Collaborative Access Team (HPCAT). The diffraction patterns from monochromatic 0.3344 and 0.4066 Å wavelength x rays were collected on a Pilatus 1M image-plate detector/PI-MAX, Princeton Instruments, which were integrated using DIOPTAS[38] into a 1D dataset. Collection times ranged between 2 and 5 s. These data were then indexed using CONOGRAPH[39] and refined with JANA2006.[40]

To allow the investigation of high-temperature transitions in Ge, several experiments were conducted making use of flattop continuous-wave laser heating techniques within diamond anvil cells using an Yb fiber laser setup for stable dual sided heating.[28] We conducted simultaneous *in situ* double-sided continuous-wave (CW) laser heating and x-ray diffraction experiments in diamond anvil cells. Laser heating results in highly localized heating of the sample both radially from the "hot spot" and in depth. As such, these large thermal gradients result in probing both crystalline and

molten samples simultaneously at high temperatures. The temperatures in all experimental runs are determined by taking the average of the black-body thermal emission from both sides of the sample; see Fig. S1 for an example of emission spectra. Thermal emission spectra were collected with a central wavelength of 700 nm with a collection time between 0.1 ms and 1 s depending on the intensity of the emitted light. The emission spectra were sampled between two and eight times per temperature step from both the up-stream and down-stream sides of the sample simultaneously. The collected emission spectra were fitted using a two parameter gray body Plank distribution,[41] corrected for the transmission function of the optical system.[42] For each set of temperatures, the mean average is used as the average temperature of the sample. The uncertainties of these temperatures were determined from the standard error on the mean of the fitted temperatures.[42] In the event of poor quality thermal emission from one side of the sample or an unreasonable thermal emission spectra due to "flashing" or a non-convergence of the fit on one side of the sample, the uncertainty of the temperature measurement was estimated to be 7% of the fitted temperature as this was determined to be a conservative estimate of the uncertainties associated with this fitting technique.[43]

B. Computational details

The computational–theoretical analysis of Ge under pressure has been performed within the Density Functional Theory (DFT) framework. Calculations have been performed using CASTEP.[44]

We have performed structural searches using AIRSS at 10, 80, and 100 GPa. Searches at 10 GPa were performed with a $4e^-$ pseudopotential. All searches used the Perdew–Burke–Ernzerhof (PBE) functional. At higher pressures, the pseudopotentials of choice included the $3d^{10}$ electrons as semicore. Searches at 10, 80, and 100 GPa with AIRSS[45] (with unit cells with up to 24 atoms) identified Ge-II ($I4_1/amd$), Ge-IV ($Imma$), Ge-V ($P6/mmm$), and Ge-VI ($Cmca$), in addition to the new Ge-VIII ($I4/mmm$). Our searches identified all structures in Table S1, as well as the proposed $I4/mmm$ structure and other competitive structures. Further computational details and the structures found can be accessed in the Edinburgh DataShare repository.[46] Overall, we relaxed almost 5000 structures.

III. RESULTS AND DISCUSSION

A. Experimental evidence of Ge phase VIII

Upon compression at ambient temperatures, there is good agreement with the previously reported phase transition pressures. Figure 2(a) shows the XRD patterns of Ge-II ($I4_1/amd$) observed in compression at room temperature[18,19] and its transition to phase IV ($Imma$) between 70 and 80 GPa,[20] and the following transition to phase V ($P6/mmm$).[21] When heating Ge-II between pressures of 56–61 GPa, as shown in Fig. 2(b), we observe changes in the diffraction pattern corresponding to a transition to the orthorhombic Ge-IV. At 56–61 GPa, the II/IV transition is observed between 1560(110) and 1850(130) K, accompanied by a pressure shift of ~2–4 GPa. The combined data constrain the II–IV phase boundary with a dP/dT of −0.014(3) GPa/K. Experimental studies on Si show the equivalent transition (Si-II and Si-XI) also having a phase boundary with a negative slope between 1050 K at 12 GPa and 300 K at 13.2 GPa.[35]
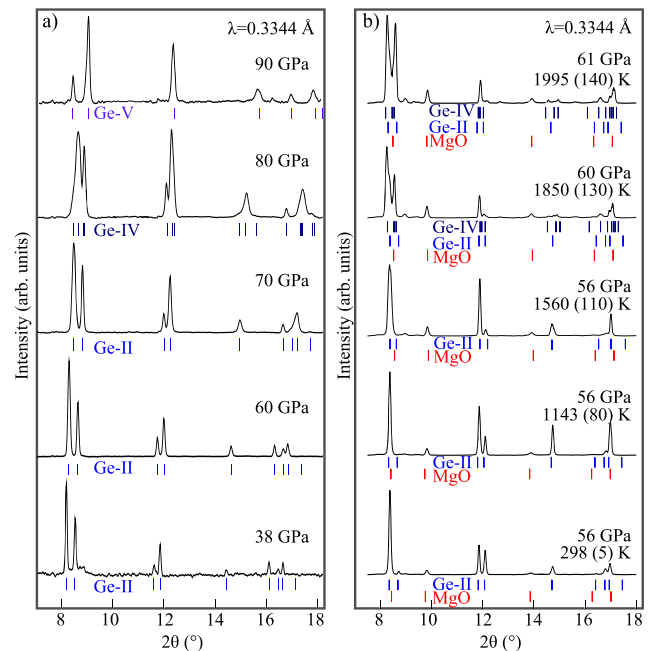

FIG. 2. (a) X-ray diffraction patterns of Ge in H_2 at 298 K upon compression to 90 GPa. (b) X-ray diffraction patterns of Ge in MgO at 56 GPa during laser heating. The phase transition is characterized by the broadening of the Ge-II peak at around 8.3°, caused by the appearance of the Ge-IV 200 peak and the growth of a triplet at around 8.8°. The pressure was determined from the Raman shift of the diamond edge[37] and the MgO equation of state (EOS).[36]

Upon laser heating Ge-IV at pressures above 64 GPa and 1600 K, we observe changes in the diffraction patterns. With the emergence of new diffraction peaks, there is a simultaneous reduction in the intensity of the Ge-IV peaks that indicate a transition to a novel phase, which we designate Ge-VIII (see Figs. 2 and 3). The transition is completely reversible and Ge-VIII reverts to Ge-IV upon cooling, see Fig. 3(b).

This new set of peaks [2D image plates in Fig. 4(a)] can be indexed to a tetragonal unit cell with lattice parameters of $a = 2.978(5)$ Å and $c = 2.732(3)$ Å [Figs. 4(b)–4(d)]. Analysis of systematic absences within the diffraction patterns indicated an absence of glide and screw symmetry elements. The highest symmetry space group consistent with this analysis is $I4/mmm$. We observe the same transition when the experiment is conducted using MgO and H_2 as pressure-transmitting media, indicating that this transition is not due to the formation of Ge compounds. Figures 4(c) and 4(e) show the Le Bail refinements in different experimental runs, using MgO and H_2 as PTM, respectively. We observe the same transition in both the cases, validating the evaluation of Ge-VIII. Due to the overlap of Ge-VIII and MgO (202) Bragg peaks, combined with poor crystallinity around the transition temperature, our analysis was limited to Le Bail refinements in combination with first-principles calculations. As shown in Fig. 4(c), fitting an $I4/mmm$ structure with lattice parameters $a = 2.978(5)$ Å and $c = 2.732(3)$ Å along with the expected contributions from Ge-IV and MgO provides a high quality fit. These lattice parameters give a volume of 12.11(1) Å³/atom. Comparing this with Ge-IV lattice parameters of $a = 4.577(4)$ Å,
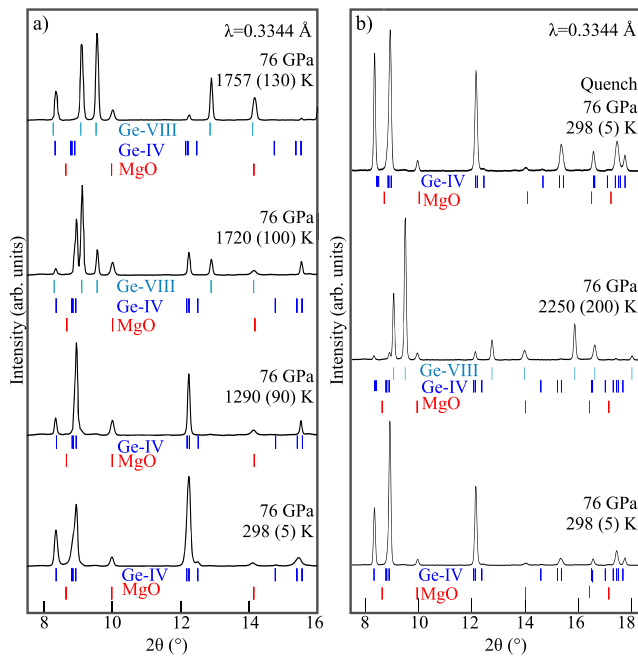
FIG. 3. (a) High-pressure, high-temperature x-ray diffraction patterns of Ge in MgO at 76 GPa, showing the IV/VIII transition. (b) X-ray diffraction patterns of Ge in MgO at 76 GPa before, during, and after laser heating, demonstrating the reversibility of the Ge-IV/VIII transition with temperature. The pressure was calculated from the positions of the MgO using its EOS.[36]

b = 4.376(3) Å , and c = 2.4731(15) Å gives an atomic volume of 12.38(1) Å^3/atom, which is approximately constant across the transition indicating a potential displacive transition and a Z value of 2. Using this value of Z = 2, two potential atomic positions ($2a$ and $2b$) are possible for space group $I4/mmm$. By comparing the collected diffraction profile to a simulated ideal powder pattern, shown in Figs. 4(c) and 4(d), there is a distinct similarity between the intensity profiles of the collected data and the ideal powder with atoms occupying the $2a$ Wyckoff site (0,0,0).

To our knowledge, Ge-VIII represents the first high-temperature phase to be discovered in the group-XIV elements at high-pressure, other than the diamond form of carbon. Interestingly, tin (Sn), directly below Ge in group-XIV, also exhibits a structural transition from $I4_1/amd$ (Sn-I) to $I4/mmm$ (Sn-III) at 9.2 GPa and 300 K.[47,48] As group-XIV elements seem to follow a parallel phase template, it would be expected that the remaining elements of the group also adopt the $I4/mmm$ at different and yet to be explored conditions. Isotropy subgroup distortion analysis[49] indicates that a direct displacive transition is possible between the high-temperature parent Ge-VIII ($I4/mmm$) and low-temperature daughter Ge-IV phases ($Imma$). Consistent with a displacive transition, transformation occurs via a mode with N_2^- symmetry involving anti-parallel displacements of Ge atoms, suggesting a possible mechanism for this transition.

B. Density functional theory and Ge phase VIII

To further understand the stability regime of Ge-VIII, we have analyzed the Ge structural energy landscape using DFT with the
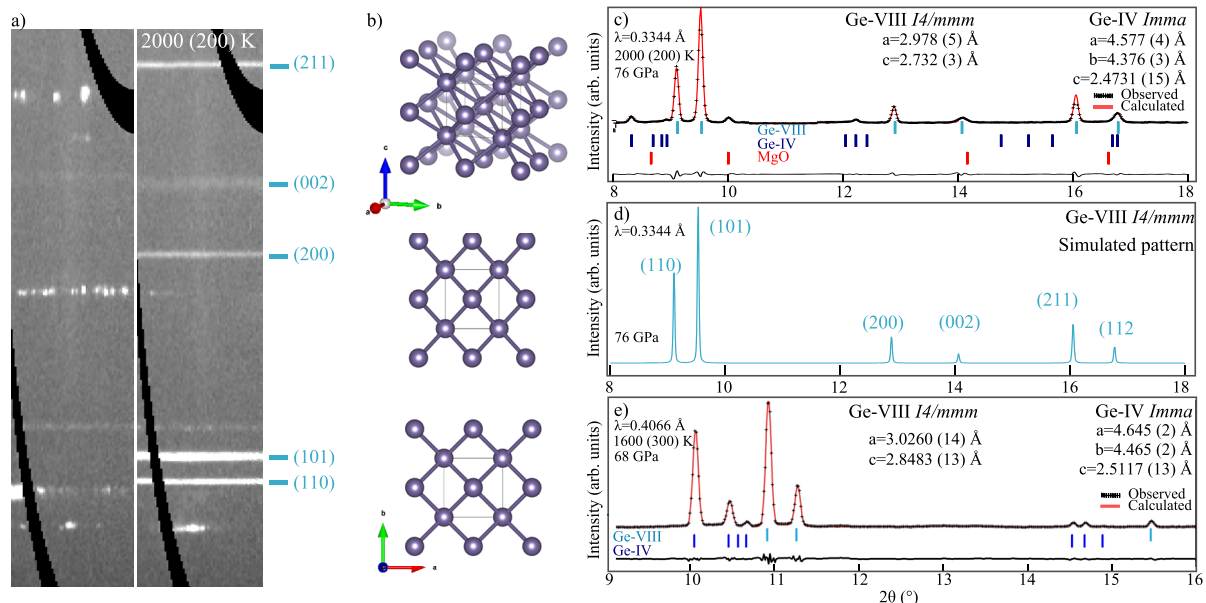

FIG. 4. (a) 2D image plates at room temperature (left) and at 2000 (200) K (right) at 76 GPa. The contributions to the diffraction image plate from Ge-VIII are indicated by the blue lines, along with their corresponding Bragg peak indices. Spotty features are from Ge-IV and Debeye–Scherrer rings are from MgO. (b) Ball and stick model of the determined atomic structure associated with the Ge-VIII phase at 76 GPa and 1750 K. (c) Le Bail refinement of Ge-VIII in MgO at 76 GPa and 2000 K. (d) Simulated pattern of the structure, with Ge atoms occupying the 2a Wyckoff position. (e) Le Bail refinement of Ge-VIII in H$_2$ at 68 GPa and 1600(300) K.
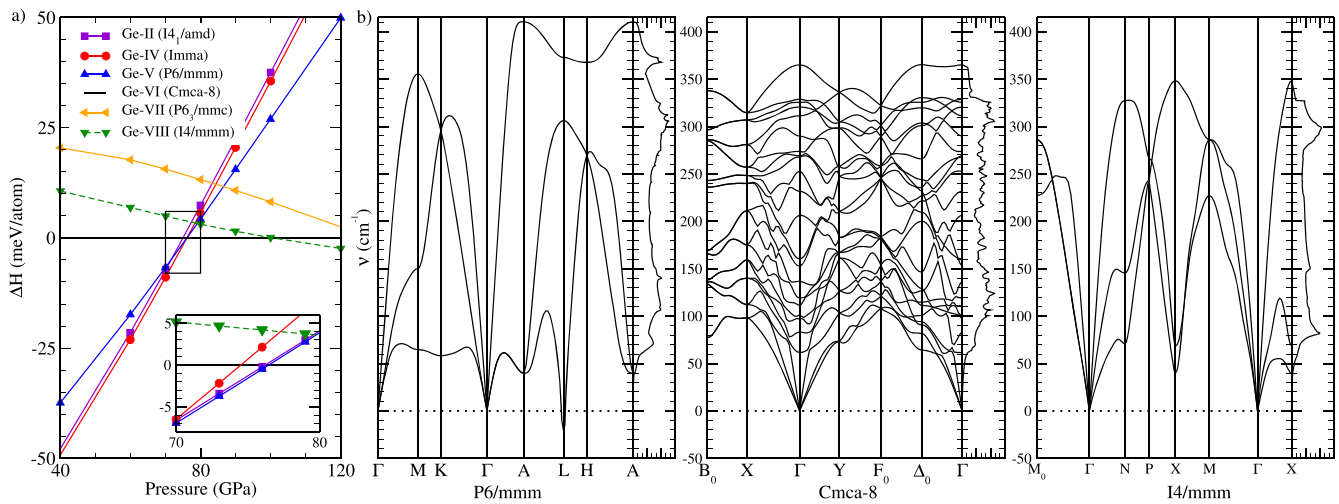
FIG. 5. (a) DFT-PBE enthalpy difference of the most competitive structures at 80 GPa, relative to Ge-V *P6/mmm*-1. Inset: 70–80 GPa region using the PBEsol. (b) Phonon dispersions and densities of states for various structures of Ge at 80 GPa. In *I4/mmm*, the lower maximum and higher relative weight below 100 cm⁻¹ indicates a high-temperature competitive free energy.
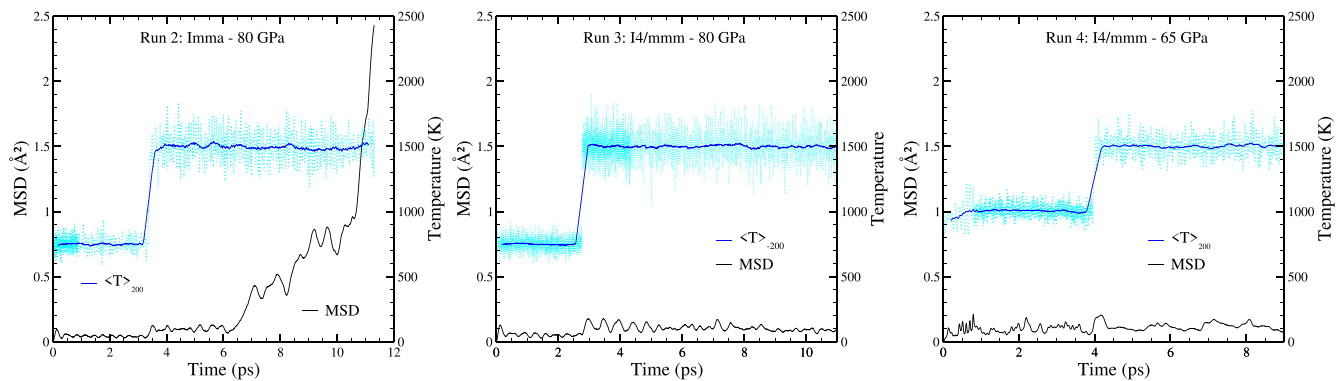

FIG. 6. Calculated mean square displacement (MSD) (black) and temperature (cyan) of (left) the 80 GPa MD run of *Imma*-2 Ge-IV at 80 GPa. MSD fluctuations appear 2 ps after increasing the temperature to 1500 K. The structure melts 10 ps after switching to an NPT ensemble. (Middle) MSD of *I4/mmm* Ge at 65 GPa. (Right) MSD of *I4/mmm* Ge at 80 GPa.

Perdew–Burke–Ernzerhof (PBE) functional[50] and ultrasoft pseudopotentials[51] as implemented in CASTEP[44] 18.1.

Calculations are detailed in the supplementary material and the raw data, including the search setup, DFT enthalpies and phonons, and *ab initio* molecular dynamics (MD) runs, are accessible from the Edinburgh DataShare repository.[46]

The enthalpies of the most competitive structures have been computed to a higher degree of accuracy, with the C18 pseudopotential, and k-point spacing denser than 0.025 Å⁻¹. Figure 5(a) shows the evolution of the enthalpy difference of these structures with pressure indicating that all of these structures are extremely competitive between 60 and 90 GPa. This has been done with the PBE functional (475 eV cutoff) and the PBEsol functional (600 eV). The transition pressures are almost identical:

PBE:

$$Imma \xrightarrow{75.9\ GPa} P6/mmm \xrightarrow{76.2\ GPa} Cmca \xrightarrow{100.5\ GPa} I4/mmm,$$

PBEsol:

$$Imma \xrightarrow{68.7\ GPa} P6/mmm \xrightarrow{76.5\ GPa} Cmca.$$

We considered obtaining a *P–T* phase diagram using the quasi-harmonic approximation. This is complicated due to the second-order nature of the phase transitions and their vicinity to the region of interest. The presence of soft phonons is likely to render the high-temperature region in which our interest is very unreliable. Instead, we performed a series of phonon calculations with QUANTUM-ESPRESSO

using Density Functional Perturbation Theory (DFPT) to assess the dynamics of the system. Figures 5(b)–5(d) show the phonons of $P6/mmm$, $Cmca - 8$, and $I4/mmm$ at 80 GPa.

The high-temperature stability of the $Imma$ phase, which is the experimental one at 300 K between 75 and 85 GPa, and the new $I4/mmm$ candidate was probed using *ab initio* molecular dynamics (AIMD). We chose a time step of 2 fs, which would sample the highest frequency phonon mode in Fig. 5(b) over 40 times per oscillation. The initial $Imma$ configuration was a $2\sqrt{2} \times 2\sqrt{2} \times 2$ supercell of the conventional cell, with 128 atoms. The initial $I4/mmm$ configuration was a $2 \times 2 \times 2$ supercell of the conventional cell, also containing 128 atoms. Both supercells have similar volumes and lattice parameters at 80 GPa. MD simulations were ran in CASTEP 18.1, with the QC5 pseudopotential, a 300 eV cutoff, and a $2 \times 2 \times 2$ k-point grid with a 0.3 eV smearing width. In total, four distinct MD runs were performed.

In Run 1, Ge-$Imma$ at 80 GPa was stabilized for 1 ps at 300 K using the NVT ensemble. The ensemble was then changed to NPT, and the cell was further stabilized for another 1.5 ps. The cell was then heated up to 1500 K. However, the system melted within 0.1 ps, being comparatively too fast to be represented.

In Run 2 (Fig. 6 left), Ge-$Imma$, at the average 300 K and 80 GPa lattice parameters, was stabilized on NVT at 750 K for 3.5 ps. The cell was then heated up to 1500 K, using a thermostat chain five times longer than in run 1. The system was kept on these conditions, using the NVT ensemble, for a further 6.5 ps. After 3 ps at 1500 K, there is a large jump in the mean square displacement (MSD). This is related to anti-parallel displacements in the atomic positions and a potential phase transition. This is shown in Fig. 6. To test if the new structure is stable, the cell was relaxed under the NPT ensemble. The system melts, however, within 1 ps.

In Run 3 (Fig. 6 middle), Ge-$I4/mmm$ at 80 GPa was stabilized at 750 K on the NVT ensemble for 2.75 ps. The temperature was then increased to 1500 K as in Run 2. The ensemble was changed to NPT at 10 ps. No phase transition was seen for 3.5 ps at 1500 K.

In Run 4 (Fig. 6 right), Ge-$I4/mmm$ at 65 GPa was stabilized at 300 K on the NPT ensemble for 1 ps. The temperature was then increased to 1000 K and run for 4 ps. The temperature was again increased to 1500 K for a further 3 ps. No substantial changes to the structure were seen during the simulation.

In summary, within DFT, $Imma$ Ge-IV is not stable at 80 GPa and 1500 K; at these conditions, there must be a transition to $I4/mmm$ Ge-VIII before melting at higher temperatures.

C. Further extensions of the Ge phase diagram

At pressures above 86 GPa at ambient temperature, Ge-IV transforms to hexagonal Ge-V and Ge-VI at around 100 GPa, shown in Fig. 7. While heating phase V, we still see the transition to phase VIII above 1700 K [Fig. 7(a)], but heating phase VI at 110 GPa shows no indication of the transition to phase VIII [Fig. 7(b)]. These results suggest that both Ge-IV–V and Ge-VIII–V phase boundaries are near vertical. The combined data consequently imply the existence of a IV–V–VIII triple point at 1600 K and 86 GPa.

We also observe evidence of melting in some of our heating cycles: in addition to a decrease in intensity of the corresponding Bragg peaks of the solid phase, there is an emergence of diffuse scattering from liquid Ge,[52] which is shown in Fig. S2. By subtracting
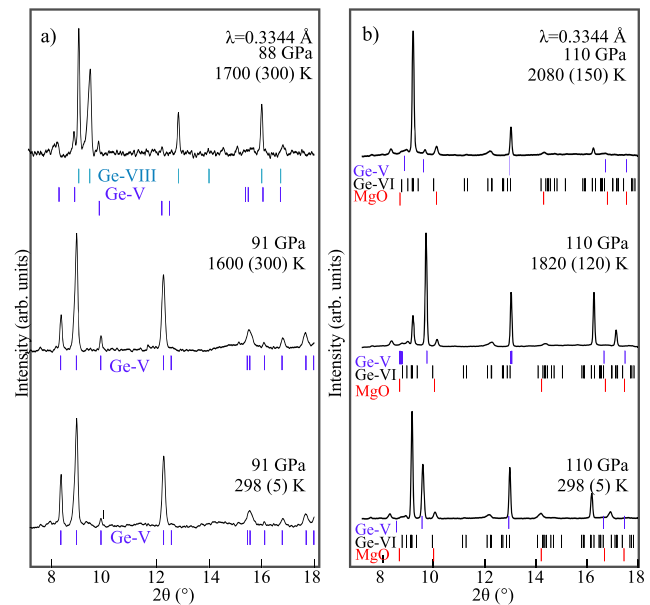

FIG. 7. (a) X-ray diffraction patterns of Ge in H_2 at 91 GPa during laser heating. The pressure was measured with diamond edge before and after heating.[37] (b) X-ray diffraction patterns of Ge in MgO at 110 GPa during laser heating. The pressure determined by MgO EOS.[36]

the background function of the room temperature pattern from the high-temperature pattern, the diffuse liquid scattering can be readily extracted.[28,53] As shown in Figs. S2 and S3, at 44 GPa, we detect Ge-II melting above 1500 K (Fig. 1). At pressures of 60 GPa, we identify Ge-IV melt around 1900 K, slightly higher than what would be expected from extrapolations of the Ge-II melt line and implying an increase in the gradient above the II–IV–liquid triple point.[28] Heating Ge-VIII at pressures of 68 GPa (Figs. S2 and S3), we see evidence of melting at 2700 K, suggesting another change in gradient after the IV–VIII–liquid triple point. In all further heating runs above 68 GPa, no evidence of melting was observed (Fig. 7), with Ge-VI remaining solid at 110 GPa and 2080 K. The melting line of Ge has been previously determined up to pressures of 37 GPa,[28] and we extend it up to 68 GPa.

IV. CONCLUSIONS

The extended phase diagram of germanium based on our results is presented in Fig. 1. Our experiments show that the $I4/mmm$ structure that we assign as Ge-VIII is reached through heating $Imma$ Ge-IV. The former is only stable at high temperatures, reversing back to Ge-IV after temperature quenching. Contrary to Ge-IV, Ge-V and Ge-VI remain stable at high temperatures, confining Ge-VIII to a narrow range of P–T space. To our knowledge, Ge-VIII represents the first high-temperature phase to be discovered in the group-XIV elements at high pressure, other than the diamond form of carbon. Similarities between the pressure and temperature phase transitions among the group XIV elements pose an interesting question as to whether an $I4/mmm$ phase could also be observed in Si. Experimental studies on Si show the equivalent transition to Ge-II–IV, which would be Si-II. Si-XI also has a phase boundary with

a negative slope between 1050 K at 12 GPa and 300 K at 13.2 GPa.[35] In Si, the pathway toward an equivalent Ge-VIII phase would require heating Si-XI, which exists in a very narrow pressure range between 13.2 and 15.4 GPa.[22,23] It is possible that due to a very narrow window at which the phase could exist, the Si-$I4/mmm$ configuration might have been overlooked.[35] Nevertheless, the discovery of Ge-VIII suggests that further high-temperature dense phases could exist in the group-XIV elements.[55]

SUPPLEMENTARY MATERIAL

The supplementary material contains a table with the phase boundaries of Si and Ge, some examples of our temperature measurements from black-body emission, and Ge XRD image plates and diffuse scattering during melting.

ACKNOWLEDGMENTS

DATA AVAILABILITY

The data that support the findings of this study are available from the corresponding author upon reasonable request. Molecular dynamics runs are available in the Edinburgh DataShare at https://datashare.is.ed.ac.uk/handle/10283/3193.

REFERENCES

[1]D. Erskine, Y. Y. Peter, K.-J. Chang, and M. L. Cohen, "Superconductivity and phase transitions in compressed Si to 45 GPa," Phys. Rev. Lett. **57**, 2741 (1986).

[2]Y. K. Vohra, K. E. Brister, S. Desgreniers, A. L. Ruoff, K.-J. Chang, and M. L. Cohen, "Phase-transition studies of germanium to 1.25 mbar," Phys. Rev. Lett. **56**, 1944 (1986).

[3]J. L. Martins and M. L. Cohen, "Superconductivity in primitive hexagonal germanium," Phys. Rev. B **37**, 3304 (1988).

[4]D. Selli, I. A. Baburin, R. Martoňák, and S. Leoni, "Novel metastable metallic and semiconducting germaniums," Sci. Rep. **3**, 1466 (2013).

[5]L. Vincent, G. Patriarche, G. Hallais, C. Renard, C. Gardès, D. Troadec, and D. Bouchier, "Novel heterostructured Ge nanowires based on polytype transformation," Nano Lett. **14**, 4828–4836 (2014).

[6]A. Lazicki, J. Rygg, F. Coppari, R. Smith, D. Fratanduono, R. Kraus, G. Collins, R. Briggs, D. Braun, D. Swift *et al.*, "X-ray diffraction of solid tin to 1.2 TPa," Phys. Rev. Lett. **115**, 075502 (2015).

[7]R. Briggs, D. Daisenberger, O. Lord, A. Salamat, E. Bailey, M. Walter, and P. McMillan, "High-pressure melting behavior of tin up to 105 GPa," Phys. Rev. B **95**, 054102 (2017).

[8]S. J. Turneaure, S. M. Sharma, and Y. Gupta, "Nanosecond melting and recrystallization in shock-compressed silicon," Phys. Rev. Lett. **121**, 135701 (2018).

[9]E. E. McBride, A. Krygier, A. Ehnes, E. Galtier, M. Harmand, Z. Konôpková, H. J. Lee, H.-P. Liermann, B. Nagler, A. Pelka *et al.*, "Phase transition lowering in dynamically compressed silicon," Nat. Phys. **15**, 89–94 (2019).

[10]R. Li, J. Liu, D. Popov, C. Park, Y. Meng, and G. Shen, "Experimental observations of large changes in electron density distributions in β-Ge," Phys. Rev. B **100**, 224106 (2019).

[11]H. J. Queisser, *The Conquest of the Microchip* (Harvard University Press, 1990).

[12]C. L. Claeys and E. E. Simoen, *Germanium-Based Technologies: From Materials to Devices* (Elsevier, 2007), p. 449.

[13]H. Katzke, U. Bismayer, and P. Tolédano, "Theory of the high-pressure structural phase transitions in Si, Ge, Sn, and Pb," Phys. Rev. B **73**, 134105 (2006).

[14]H. Olijnyk, S. K. Sikka, and W. B. Holzapfel, "Structural phase transitions in Si and Ge under pressures up to 50 GPa," Phys. Lett. A **103**, 137–140 (1984).

[15]L. J. Vandeperre, F. Giuliani, S. J. Lloyd, and W. J. Clegg, "The hardness of silicon and germanium," Acta Mater. **55**, 6307–6315 (2007).

[16]R. J. Nelmes, M. I. McMahon, N. G. Wright, D. R. Allan, H. Liu, and J. S. Loveday, "Structural studies of III–V and group IV semiconductors at high pressure," J. Phys. Chem. Solids **56**, 539–543 (1995).

[17]J. Z. Hu, L. D. Merkle, C. S. Menoni, and I. L. Spain, "Crystal data for high-pressure phases of silicon," Phys. Rev. B **34**, 4679–4684 (1986).

[18]C. S. Menoni, J. Z. Hu, and I. L. Spain, "Germanium at high pressures," Phys. Rev. B **34**, 362–368 (1986).

[19]G. A. Voronin, C. Pantea, T. W. Zerda, J. Zhang, L. Wang, and Y. Zhao, "*In situ* x-ray diffraction study of germanium at pressures up to 11 GPa and temperatures up to 950 K," J. Phys. Chem. Solids **64**, 2113–2119 (2003).

[20]X.-J. Chen *et al.*, "β-tin→*Imma*→sh phase transitions of germanium," Phys. Rev. Lett. **106**, 135502-1–135502-4 (2011).

[21]R. J. Nelmes, H. Liu, S. A. Belmonte, J. S. Loveday, M. I. McMahon, D. R. Allan, D. Häusermann, and M. Hanfland, "Imma phase of germanium at 80 GPa," Phys. Rev. B **53**, R2907–R2909 (1996).

[22]M. I. McMahon and R. J. Nelmes, "New high-pressure phase of Si," Phys. Rev. B **47**, 8337–8340 (1993).

[23]M. I. McMahon, R. J. Nelmes, N. G. Wright, and D. R. Allan, "Pressure dependence of the *Imma* phase of silicon," Phys. Rev. B **50**, 739–743 (1994).

[24]J. C. Jamieson, "Crystal structures at high pressures of metallic modifications of silicon and germanium," Science **139**, 762–764 (1963).

[25]M. Hanfland, U. Schwarz, K. Syassen, and K. Takemura, "Crystal structure of the high-pressure phase silicon VI," Phys. Rev. Lett. **82**, 1197–1200 (1999).

[26]K. Takemura, U. Schwarz, K. Syassen, M. Hanfland, N. E. Christensen, D. L. Novikov, and I. Loa, "High-pressure Cmca and hcp phases of germanium," Phys. Rev. B **62**, R10603–R10606 (2000).

[27]S. J. Duclos, Y. K. Vohra, and A. L. Ruoff, "hcp to fcc transition in silicon at 78 GPa and studies to 100 GPa," Phys. Rev. Lett. **58**, 775–777 (1987).

[28]V. B. Prakapenka, A. Kubo, A. Kuznetsov, A. Laskin, O. Shkurikhin, P. Dera, M. L. Rivers, and S. R. Sutton, "Advanced flat top laser heating system for high pressure research at GSECARS: Application to the melting behavior of germanium," High Pressure Res. **28**, 225–235 (2008).

[29]S. B. Qadri, E. F. Skelton, and A. W. Webb, "High pressure studies of Ge using synchrotron radiation," J. Appl. Phys. **54**, 3609–3611 (1983).

[30]F. P. Bundy and J. S. Kasper, "A new dense form of solid germanium," Science **139**, 340–341 (1963).

[31]Z. Zhao, H. Zhang, D. Y. Kim, W. Hu, E. S. Bullock, and T. A. Strobel, "Properties of the exotic metastable ST12 germanium allotrope," Nat. Commun. **8**, 13909 (2017).

[32]L. Q. Huston, B. C. Johnson, B. Haberl, S. Wong, J. S. Williams, and J. E. Bradby, "Thermal stability of simple tetragonal and hexagonal diamond germanium," J. Appl. Phys. **122**, 175108 (2017).

[33]R. J. Nelmes, M. I. McMahon, N. G. Wright, D. R. Allan, and J. S. Loveday, "Stability and crystal structure of BC8 germanium," Phys. Rev. B **48**, 9883–9886 (1993).

[34]C. H. Bates, F. Dachille, and R. Roy, "High-pressure transitions of germanium and a new high-pressure form of germanium," Science **147**, 860–862 (1965).

[35]A. Kubo, Y. Wang, C. E. Runge, T. Uchida, B. Kiefer, N. Nishiyama, and T. S. Duffy, "Melting curve of silicon to 15 GPa determined by two-dimensional

angle-dispersive diffraction using a Kawai-type apparatus with x-ray transparent sintered diamond anvils," J. Phys. Chem. Solids **69**, 2255–2260 (2008).

[36] S. Speziale, C.-S. Zha, T. S. Duffy, R. J. Hemley, and H.-K. Mao, "Quasi-hydrostatic compression of magnesium oxide to 52 GPa: Implications for the pressure-volume-temperature equation of state," J. Geophys. Res. **106**, 515–528, https://doi.org/10.1029/2000jb900318 (2001).

[37] Y. Akahama and H. Kawamura, "Pressure calibration of diamond anvil Raman gauge to 310 GPa," J. Appl. Phys. **100**, 043516 (2006).

[38] C. Prescher and V. B. Prakapenka, "*DIOPTAS*: A program for reduction of two-dimensional x-ray diffraction data and data exploration," High Pressure Res. **35**, 223–230 (2015).

[39] R. Oishi-Tomiyasu, "Robust powder auto-indexing using many peaks," J. Appl. Crystallogr. **47**, 593–598 (2014).

[40] V. Petříček, M. Dušek, and L. Palatinus, "Crystallographic computing system JANA2006: General features," Z. Kristallogr.-Cryst. Mater. **229**, 345–352 (2014).

[41] G. Shen, M. L. Rivers, Y. Wang, and S. R. Sutton, "Laser heated diamond cell system at the advanced photon source for *in situ* x-ray measurements at high pressure and temperature," Rev. Sci. Instrum. **72**, 1273–1282 (2001).

[42] R. A. Fischer, A. J. Campbell, O. T. Lord, G. A. Shofner, P. Dera, and V. B. Prakapenka, "Phase transition and metallization of FeO at high pressures and temperatures," Geophys. Res. Lett. **38**, L24301, https://doi.org/10.1029/2011gl049800 (2011).

[43] S. Deemyad, A. N. Papathanassiou, and I. F. Silvera, "Strategy and enhanced temperature determination in a laser heated diamond anvil cell," J. Appl. Phys. **105**, 093543 (2009).

[44] S. J. Clark, M. D. Segall, C. J. Pickard, P. J. Hasnip, M. I. Probert, K. Refson, and M. C. Payne, "First principles methods using CASTEP," Z. Kristallogr.-Cryst. Mater. **220**, 567–570 (2005).

[45] C. J. Pickard and R. J. Needs, J. Phys.: Condens. Matter **23**, 053201 (2011).

[46] M. Martinez-Canales and C. J. Pickard, Raw DFT data for "High-temperature phase transitions in dense germanium" [dataset] (University of Edinburgh, School of Physics & Astronomy, 2021). https://doi.org/10.7488/ds/3019.

[47] J. D. Barnett, V. E. Bean, and H. T. Hall, "X-ray diffraction studies on tin to 100 kilobars," J. Appl. Phys. **37**, 875–877 (1966).

[48] A. Salamat, R. Briggs, P. Bouvier, S. Petitgirard, A. Dewaele, M. E. Cutler, F. Cora, D. Daisenberger, G. Garbarino, and P. F. McMillan, "High-pressure structural transformations of Sn up to 138 GPa: Angle-dispersive synchrotron x-ray diffraction study," Phys. Rev. B **88**, 104104 (2013).

[49] M. Müller, R. E. Dinnebier, A.-C. Dippel, H. T. Stokes, and B. J. Campbell, "A symmetry-mode description of rigid-body rotations in crystalline solids: A case study of $Mg(H_2O)_6RbBr_3$," J. Appl. Crystallogr. **47**, 532–538 (2014).

[50] J. P. Perdew, K. Burke, and M. Ernzerhof, "Generalized gradient approximation made simple," Phys. Rev. Lett. **77**, 3865–3868 (1996).

[51] D. Vanderbilt, "Soft self-consistent pseudopotentials in a generalized eigenvalue formalism," Phys. Rev. B **41**, 7892–7895 (1990).

[52] A. Salamat, R. A. Fischer, R. Briggs, M. I. McMahon, and S. Petitgirard, "*In situ* synchrotron x-ray diffraction in the laser-heated diamond anvil cell: Melting phenomena and synthesis of new materials," Coord. Chem. Rev. **277-278**, 15–30 (2014).

[53] J. Kōga, H. Okumura, K. Nishio, T. Yamaguchi, and F. Yonezawa, "Simulational analysis of the local structure in liquid germanium under pressure," Phys. Rev. B **66**, 064211 (2002).

[54] V. V. Brazhkin, A. G. Lyapin, S. V. Popova, and R. N. Voloshin, "Nonequilibrium phase transitions and amorphization in Si, Si/GaAs, Ge, and Ge/GaSb at the decompression of high-pressure phases," Phys. Rev. B **51**, 7549 (1995).

[55] C. Claeys and E. Simoen, *Germanium-Based Technologies: From Materials to Devices* (Elsevier, 2011).